

One-loop corrections to the neutrino in the N-B-LSSM

Shuang Di^{1,2,3}, Shu-Min Zhao^{1,2,3*}, Ming -Yue Liu^{1,2,3},

Xing-Yu Han^{1,2,3}, Song Gao^{1,2,3}, Xing-Xing Dong^{1,2,3,4†}

¹ *Department of Physics, Hebei University, Baoding 071002, China*

² *Hebei Key Laboratory of High-precision Computation and Application of Quantum Field Theory, Baoding, 071002, China*

³ *Hebei Research Center of the Basic Discipline for Computational Physics, Baoding, 071002, China and*

⁴ *Departamento de Fisica and CFTP, Instituto Superior Técnico, Universidade de Lisboa, Av.Rovisco Pais 1,1049-001 Lisboa, Portugal*

(Dated: July 8, 2025)

Abstract

In this paper, we study one-loop corrections to the neutrino mass matrix in the N-B-LSSM. We obtain the N-B-LSSM from the $U(1)$ extension of the minimal supersymmetric standard model(MSSM). By adding three generation right-handed neutrino superfields and three Higgs singlets, the model generates tiny neutrino masses at the tree level through the first type seesaw mechanism. However, one-loop corrections are essential for understanding neutrino masses and mixing angles. We calculate the neutrino mass variance and mixing angle from both normal order neutrino mass spectrum and inverse order neutrino mass spectrum. This study provides new theoretical support for exploring the mechanism of neutrino mass generation in the supersymmetric model and provides clues for exploring new physics beyond the Standard Model (SM).

PACS numbers:

Keywords: the neutrino mass, N-B-LSSM, the one-loop corrections, new physics.

* zhaosm@hbu.edu.cn

† dongxx@hbu.edu.cn

I. INTRODUCTION

The Standard Model (SM) of particle physics, despite its tremendous successes, there remains phenomena that cannot be explained. For instance, the SM fails to account for neutrino masses and their mixing patterns[1–4]. The masses and mixing patterns of neutrinos constitute a critical research area in particle physics, as they hold profound implications for cosmology and the fundamental understanding of particle interactions.

Recent experimental data, such as neutrino oscillation experiments released by the Daya Bay Laboratory in 2024[5], have further promoted studies on neutrino masses and lepton flavor violating processes[6–8]. These data not only provide precise measurements of neutrino mixing angles but also impose new constraints on the upper and lower bounds of neutrino masses. Such constraints are vital for unraveling the nature of neutrinos and their role in the universe. The present 3σ limits for the neutrino experiment data are[9]

$$\begin{aligned} 0.0198 &\leq \sin^2 \theta_{13} \leq 0.024, \\ 0.268 &\leq \sin^2 \theta_{12} \leq 0.346, \\ 0.385 &\leq \sin^2 \theta_{23} \leq 0.644, \\ 6.99 \times 10^{-5} &\leq \Delta m_{\odot}^2 \leq 8.07 \times 10^{-5}, \\ 2.371 \times 10^{-3} &\leq \Delta m_A^2(\text{NO}) \leq 2.539 \times 10^{-3}, \\ -2.679 \times 10^{-3} &\leq \Delta m_A^2(\text{IO}) \leq -2.505 \times 10^{-3}. \end{aligned}$$

Based on the MSSM, the minimal supersymmetric extension of the SM with local B-L gauge symmetry (N-B-LSSM) is obtained by extending the gauge symmetry group to $SU(3)_C \times SU(2)_L \times U(1)_Y \times U(1)_{B-L}$ [10]. The N-B-LSSM introduces three additional Higgs singlets and three generation right-handed neutrinos on the basis of the MSSM. It generates the tiny mass of light neutrinos through the seesaw mechanism. And it provides an effective solution to the μ problem that the MSSM cannot resolve. In the N-B-LSSM, the Higgs singlet S acquires a non-zero vacuum expectation value (VEV) $\frac{v_S}{\sqrt{2}}$, and its superpotential $\lambda S H_u H_d$ induces an effective μ term $\mu = \frac{\lambda v_S}{\sqrt{2}}$. This mechanism replaces the $\mu H_u H_d$ term in the MSSM and alleviates the μ problem. With the introduction of three Higgs singlets, the neutral CP-even Higgs mass matrix is extended to a 5×5 dimension, providing a more natural explanatory framework for the 125 GeV Higgs mass. This work assumes R-parity conservation. In the N-B-LSSM, R-parity is automatically conserved (without the need for manual addition), as the conservation law is defined as: $R_p = (-1)^{3(B-L)+2S}$. Other

terms in superpotential are allowed. For convenience, they are not considered in this study, because their effects can be combined in the already present terms, and they do not have a substantial new impact on our research.

In the N-B-LSSM, we have discussed certain two-loop contributions to muon anomalous magnetic dipole moment, lepton flavour-violating decays $l_j \rightarrow l_i \gamma$, $l_j \rightarrow 3l_i$ and $\mu \rightarrow e + q\bar{q}$, but the neutrino mass problem has not yet been studied[10]. In this paper, we study the neutrino mass correction problem under the N-B-LSSM, neutrinos acquire tiny masses at tree level through the seesaw mechanism[11–14], facilitated by the introduction of right-handed neutrino fields. However, the one-loop corrections are crucial not only for neutrino mass and mixing[15, 16] but also significantly impact other physical processes. Loop corrections play essential roles in lepton flavor violating processes such as the radiative decays $l_j \rightarrow l_i \gamma$ ($i, j = 1, 2, 3, i \neq j$)[8] with zero tree-level contribution. Neutrinos have tiny masses, which implies lepton flavor violation. Therefore, we take into account the important one-loop corrections in this work. Our corrections arise from various sources, including virtual slepton-chargino, sneutrino-neutralino, and Higgs-charged lepton loops. The inclusion of one-loop effects is essential to match the precise experimental data on neutrino oscillations, which provide stringent constraints on the neutrino mass squared differences and mixing angles.

In Ref.[17], the authors discuss the supersymmetric neutrino mass under the one-loop approximation using the on-shell renormalization scheme without taking into account lepton number conservation and R-parity. There are also some work related to the mass and mixing of neutrinos[18–21]. This paper focuses on the one-loop corrections to the neutrino mass matrix in the N-B-LSSM. We employ the method of mass eigenstates to calculate these corrections and analyze their impact on the neutrino mass spectrum and mixing angles. Our study aims to explore the parameter space of the N-B-LSSM that is consistent with the current neutrino oscillation data. By doing so, we aim to shed light on the underlying mechanisms of neutrino mass generation and to provide insights into the new physics beyond the SM.

The structure of this paper is as follows: In Sec.II, we briefly review the N-B-LSSM and its key features relevant to neutrino mass generation. Sec.III details the calculation of one-loop corrections to the neutrino mass matrix. In Sec.IV, we present our numerical results and discuss the implications for the neutrino mass spectrum and mixing angles. Finally, the

conclusion are given out in Sec.V.

II. THE N-B-LSSM

N-B-LSSM is the $U(1)_{B-L}$ extension of MSSM, and the local gauge group is $SU(3)_C \times SU(2)_L \times U(1)_Y \times U(1)_{B-L}$ [22]. In order to obtain the N-B-LSSM, new superfields are added to the MSSM, including three Higgs singlets $\hat{\chi}_1$, $\hat{\chi}_2$, \hat{S} and right-handed superfields $\hat{\nu}_i$. Through the seesaw mechanism, the minuteness of the neutrino mass can be naturally explained. The neutral CP-even scalar fields of H_u , H_d , χ_1 , χ_2 and S mix into a 5×5 mass squared matrix. The superpotential in N-B-LSSM is expressed as

$$W = -Y_d \hat{d} \hat{q} \hat{H}_d - Y_e \hat{e} \hat{l} \hat{H}_d - \lambda_2 \hat{S} \hat{\chi}_1 \hat{\chi}_2 + \lambda \hat{S} \hat{H}_u \hat{H}_d \\ + \frac{\kappa}{3} \hat{S} \hat{S} \hat{S} + Y_u \hat{u} \hat{q} \hat{H}_u + Y_X \hat{\nu} \hat{\chi}_1 \hat{\nu} + Y_\nu \hat{\nu} \hat{l} \hat{H}_u. \quad (1)$$

Under this model, $Y_{u,d,e,\nu,\chi}$ in the superpotential denote the Yukawa coupling coefficients. While λ , λ_2 and κ are dimensionless couplings constant. $\hat{\chi}_1$, $\hat{\chi}_2$, \hat{S} are three Higgs singlets.

The vacuum expectation values(VEVs) of the Higgs superfields H_u , H_d , χ_1 , χ_2 and S are presented by v_u , v_d , v_η , $v_{\bar{\eta}}$ and v_S respectively. Two angles are defined as $\tan \beta = v_u/v_d$ and $\tan \beta_\eta = v_{\bar{\eta}}/v_\eta$. The definition of $\tilde{\nu}_L$ and $\tilde{\nu}_R$ is

$$\tilde{\nu}_L = \frac{1}{\sqrt{2}}\phi_L + \frac{i}{\sqrt{2}}\sigma_L, \quad \tilde{\nu}_R = \frac{1}{\sqrt{2}}\phi_R + \frac{i}{\sqrt{2}}\sigma_R. \quad (2)$$

The specific explicit expressions of the neutral components of the two Higgs doublets and three Higgs singlets are as follows

$$H_d^0 = \frac{1}{\sqrt{2}}\phi_d + \frac{1}{\sqrt{2}}v_d + i\frac{1}{\sqrt{2}}\sigma_d, \\ H_u^0 = \frac{1}{\sqrt{2}}\phi_u + \frac{1}{\sqrt{2}}v_u + i\frac{1}{\sqrt{2}}\sigma_u, \\ \chi_1 = \frac{1}{\sqrt{2}}\phi_1 + \frac{1}{\sqrt{2}}v_\eta + i\frac{1}{\sqrt{2}}\sigma_1, \\ \chi_2 = \frac{1}{\sqrt{2}}\phi_2 + \frac{1}{\sqrt{2}}v_{\bar{\eta}} + i\frac{1}{\sqrt{2}}\sigma_2, \\ S = \frac{1}{\sqrt{2}}\phi_S + \frac{1}{\sqrt{2}}v_S + i\frac{1}{\sqrt{2}}\sigma_S. \quad (3)$$

The soft SUSY breaking terms are shown as

$$\mathcal{L}_{soft} = \mathcal{L}_{soft}^{MSSM} - \frac{T_\kappa}{3} S^3 + \epsilon_{ij} T_\lambda S H_d^i H_u^j + T_2 S \chi_1 \chi_2$$

$$\begin{aligned}
& -T_{\chi,ik}\chi_1\tilde{\nu}_{R,i}^*\tilde{\nu}_{R,k}^* + \epsilon_{ij}T_{\nu,ij}H_u^i\tilde{\nu}_{R,i}^*\tilde{e}_{L,j} - m_\eta^2|\chi_1|^2 - m_\eta^2|\chi_2|^2 \\
& -m_S^2|S|^2 - m_{\nu,ij}^2\tilde{\nu}_{R,i}^*\tilde{\nu}_{R,j} - \frac{1}{2}(2M_{BB'}\lambda_{\tilde{B}}\tilde{B}' + \delta_{ij}M_{BL}\tilde{B}'^2) + h.c. \quad , \quad (4)
\end{aligned}$$

$\mathcal{L}_{soft}^{MSSM}$ represent the soft breaking terms of the MSSM. The parameters T_κ , T_λ , T_2 , T_χ and T_ν are trilinear coupling coefficients. The particle content and charge assignments of

TABLE I: The superfields in N-B-LSSM

| Superfields | $U(1)_Y$ | $SU(2)_L$ | $SU(3)_C$ | $U(1)_{B-L}$ |
|----------------|----------|-----------|-----------|--------------|
| \hat{q} | 1/6 | 2 | 3 | 1/6 |
| \hat{l} | -1/2 | 2 | 1 | -1/2 |
| \hat{H}_d | -1/2 | 2 | 1 | 0 |
| \hat{H}_u | 1/2 | 2 | 1 | 0 |
| \hat{d} | 1/3 | 1 | $\bar{3}$ | -1/6 |
| \hat{u} | -2/3 | 1 | $\bar{3}$ | -1/6 |
| \hat{e} | 1 | 1 | 1 | 1/2 |
| $\hat{\nu}$ | 0 | 1 | 1 | 1/2 |
| $\hat{\chi}_1$ | 0 | 1 | 1 | -1 |
| $\hat{\chi}_2$ | 0 | 1 | 1 | 1 |
| \hat{S} | 0 | 1 | 1 | 0 |

N-B-LSSM are shown in the Table I. In chiral superfield frameworks, $\hat{H}_u = (\hat{H}_u^+, \hat{H}_u^0)$ and $\hat{H}_d = (\hat{H}_d^0, \hat{H}_d^-)$ represent the MSSM-like doublet Higgs superfields. \hat{q} and \hat{l} are the doublets of quark and lepton. \hat{u} , \hat{d} , \hat{e} and $\hat{\nu}$ are the singlet up-type quark, down-type quark, charged lepton and neutrino superfields, respectively.

The gauge groups $U(1)_Y$ and $U(1)_{B-L}$ exhibit a gauge kinetic mixing effect, which can also be induced through renormalization group equations(RGEs)even with a zero value at M_{GUT} . Because the two Abelian gauge groups remain unbroken, a basis conversion can occur using a rotation matrix R ($R^T R = 1$)[23–26]. The covariant derivatives of this model can be expressed as follows

$$D_\mu = \partial_\mu - i \left(Y, B - L \right) \begin{pmatrix} g_Y & g'_{YB} \\ g'_{BY} & g'_{B-L} \end{pmatrix} \begin{pmatrix} B_\mu'^Y \\ B_\mu'^{BL} \end{pmatrix} , \quad (5)$$

in which Y and $B - L$ denote the hypercharge and the $B - L$ (baryon number minus lepton number) charge, respectively. g_B represents the gauge coupling constant of the $U(1)_{B-L}$ group. g_{YB} represents the mixing gauge coupling constant of the $U(1)_{B-L}$ group and $U(1)_Y$ group. Given that the two Abelian gauge symmetries remain unbroken, a basis transformation can be executed

$$\begin{pmatrix} g_Y & g'_{YB} \\ g'_{BY} & g'_{B-L} \end{pmatrix} R^T = \begin{pmatrix} g_1 & g_{YB} \\ 0 & g_B \end{pmatrix}. \quad (6)$$

Finally, the gauge derivative of N-B-LSSM is transformed into

$$R \begin{pmatrix} B_\mu^Y \\ B_\mu^{BL} \end{pmatrix} = \begin{pmatrix} B_\mu^Y \\ B_\mu^{BL} \end{pmatrix}. \quad (7)$$

The mass matrix for neutralino in the basis $(\lambda_{\tilde{B}}, \tilde{W}^0, \tilde{H}_d^0, \tilde{H}_u^0, \tilde{B}', \tilde{\chi}_1, \tilde{\chi}_2, S)$ is

$$m_{\chi^0} = \begin{pmatrix} M_1 & 0 & -\frac{1}{2}g_1 v_d & \frac{1}{2}g_1 v_u & M_{BB'} & 0 & 0 & 0 \\ 0 & M_2 & \frac{1}{2}g_2 v_d & -\frac{1}{2}g_2 v_u & 0 & 0 & 0 & 0 \\ -\frac{1}{2}g_1 v_d & \frac{1}{2}g_2 v_d & 0 & -\frac{1}{\sqrt{2}}\lambda v_S & -\frac{1}{2}g_{YB} v_d & 0 & 0 & -\frac{1}{\sqrt{2}}\lambda v_u \\ \frac{1}{2}g_1 v_u & -\frac{1}{2}g_2 v_u & -\frac{1}{\sqrt{2}}\lambda v_S & 0 & \frac{1}{2}g_{YB} v_u & 0 & 0 & -\frac{1}{\sqrt{2}}\lambda v_d \\ M_{BB'} & 0 & -\frac{1}{2}g_{YB} v_d & \frac{1}{2}g_{YB} v_u & M_{BL} & -g_B v_\eta & g_B v_{\bar{\eta}} & 0 \\ 0 & 0 & 0 & 0 & -g_B v_\eta & 0 & -\frac{1}{\sqrt{2}}\lambda_2 v_S & -\frac{1}{\sqrt{2}}\lambda_2 v_{\bar{\eta}} \\ 0 & 0 & 0 & 0 & g_B v_{\bar{\eta}} & -\frac{1}{\sqrt{2}}\lambda_2 v_S & 0 & -\frac{1}{\sqrt{2}}\lambda_2 v_\eta \\ 0 & 0 & -\frac{1}{\sqrt{2}}\lambda v_u & -\frac{1}{\sqrt{2}}\lambda v_d & 0 & -\frac{1}{\sqrt{2}}\lambda_2 v_{\bar{\eta}} & -\frac{1}{\sqrt{2}}\lambda_2 v_\eta & \sqrt{2}\kappa v_S \end{pmatrix} \quad (8)$$

This matrix is diagonalized by the rotation matrix N

$$N^* m_{\chi^0} N^\dagger = m_{\chi^0}^{diag}. \quad (9)$$

One can find other mass matrixes in the Appendix A.

III. ANALYTICAL FORMULA

In this section, we compute the one-loop correction to the neutrino mass under the N-B-LSSM. We perform the chiral decomposition of the fermion propagator in loop diagrams,

where $P_L = \frac{1-\gamma_5}{2}$ and $P_R = \frac{1+\gamma_5}{2}$ present chiral projection operator. The general form of the self-energy of $\nu_i - \nu_j$ is as follows

$$S_{ij}(k) = a_{ij}m_jP_L + b_{ij}m_iP_R + c_{ij}\not{k}P_L + d_{ij}\not{k}P_R. \quad (10)$$

Considering the one-loop correction, a_{ij}, b_{ij}, c_{ij} and d_{ij} are functions of k^2 . In the one-loop correction calculation, k^2 is the external neutrino momentum square, which is small. So, we perform a Taylor expansion of a_{ij}, b_{ij}, c_{ij} and d_{ij} according to k^2 . Taking into account the leading-order and next-to-leading order contributions of a_{ij}, b_{ij}, c_{ij} and d_{ij} , we obtain[17, 27]

$$\begin{aligned} a_{ij} &= a_{ij}^0 + k^2 a_{ij}^1, \\ b_{ij} &= b_{ij}^0 + k^2 b_{ij}^1, \\ c_{ij} &= c_{ij}^0 + k^2 c_{ij}^1, \\ d_{ij} &= d_{ij}^0 + k^2 d_{ij}^1. \end{aligned} \quad (11)$$

By adding counter-terms $S(k)'_{ij}$, we renormalize $S(k)_{ij}$ as

$$S_{ij}^{REN}(k) = S(k)_{ij} + a_{ij}^*m_jP_L + b_{ij}^*m_iP_R + c_{ij}^*\not{k}P_L + d_{ij}^*\not{k}P_R, \quad (12)$$

where the parts with $*$ are the counter parts. In the used renormalization scheme they are determined by the mass-shell conditions

$$\begin{aligned} S_{ij}^{REN}(k)u_j(k)|_{k^2=m_j^2} &= 0, \\ \bar{u}_i(k)S_{ij}^{REN}(k)|_{k^2=m_i^2} &= 0. \end{aligned} \quad (13)$$

From Eqs. (11)(12)(13), we can get the following solution

$$\begin{aligned} a_{ij}^* &= -a_{ij}^0 + m_i^2 b_{ij}^1 + m_i^2 c_{ij}^1 + m_i^2 m_j^2 d_{ij}^1, \\ b_{ij}^* &= -b_{ij}^0 + m_i^2 a_{ij}^1 + m_i^2 c_{ij}^1 + m_i^2 m_j^2 d_{ij}^1, \\ c_{ij}^* &= -c_{ij}^0 - m_j^2 a_{ij}^1 - m_i^2 b_{ij}^1 - (m_i^2 + m_j^2)c_{ij}^1 - m_i^2 m_j^2 d_{ij}^1, \\ d_{ij}^* &= -d_{ij}^0 - m_i^2 m_j^2 a_{ij}^1 - m_i^2 m_j^2 b_{ij}^1 - m_i^2 m_j^2 c_{ij}^1 - (m_i^2 + m_j^2)d_{ij}^1. \end{aligned} \quad (14)$$

According to Eq.(12) and Eq.(14), the renormalized self-energy can be written as

$$\begin{aligned} S_{ij}^{REN}(k) &= (m_i^2 b_{ij}^1 + m_i^2 c_{ij}^1 + m_i^2 m_j^2 d_{ij}^1 + a_{ij}^1 k^2)m_j P_L \\ &\quad + (m_j^2 a_{ij}^1 + m_j^2 c_{ij}^1 + m_i^2 m_j^2 d_{ij}^1 + b_{ij}^1 k^2)m_i P_R \end{aligned}$$

$$\begin{aligned}
& + \left(-m_j^2 a_{ij}^1 - m_i^2 b_{ij} - (m_i^2 + m_j^2) c_{ij}^1 - m_i^2 m_j^2 d_{ij}^1 + b_{ij}^1 k^2 \right) \not{k} P_L \\
& + \left(-m_i^2 m_j^2 a_{ij}^1 - m_i^2 m_j^2 b_{ij}^1 - m_i^2 m_j^2 c_{ij}^1 - (m_i^2 + m_j^2) f_{ij}^1 + d_{ij}^1 k^2 \right) \not{k} P_R \\
& = (\not{k} - m_j) \hat{S}_{ij}(k) (\not{k} - m_i),
\end{aligned} \tag{15}$$

where $\hat{S}_{ij}(k)$ is denoted as

$$\begin{aligned}
\hat{S}_{ij}(k) &= a_{ij}^1 m_j P_R + b_{ij}^1 m_i P_L + c_{ij}^1 (m_i P_L + m_j P_R + \not{k} P_R) \\
&+ d_{ij}^1 (m_i P_R + m_j P_R + \not{k} P_L).
\end{aligned} \tag{16}$$

For convenience, we have introduced some new symbols

$$\begin{aligned}
\delta Z_{ij}^L &= -m_j^2 a_{ij}^1 - m_i^2 b_{ij} - (m_i^2 + m_j^2) c_{ij}^1 - m_i^2 m_j^2 d_{ij}^1 + b_{ij}^1 k^2, \\
\delta Z_{ij}^R &= -m_i^2 m_j^2 a_{ij}^1 - m_i^2 m_j^2 b_{ij}^1 - m_i^2 m_j^2 c_{ij}^1 - (m_i^2 + m_j^2) f_{ij}^1 + d_{ij}^1 k^2, \\
\delta m_{ij}^L &= (m_i^2 b_{ij}^1 + m_i^2 c_{ij}^1 + m_i^2 m_j^2 d_{ij}^1 + a_{ij}^1 k^2) m_j, \\
\delta m_{ij}^R &= (m_j^2 a_{ij}^1 + m_j^2 c_{ij}^1 + m_i^2 m_j^2 d_{ij}^1 + b_{ij}^1 k^2) m_i,
\end{aligned} \tag{17}$$

where $\delta Z_{ij}^L(\delta Z_{ij}^R)$ is left-handed(right-handed) wave function renormalization constant. $\delta m_{ij}^L(\delta m_{ij}^R)$ is left-handed(right-handed) mass renormalization constant. They are used to construct the renormalization propagator.

Under the one-loop order, the Green's function at two points is expressed as

$$\begin{aligned}
\Gamma_{ij}(k) &= (\not{k} - m_i^{tr}) \delta_{ij} + S_{ij}^{REN}(k) \\
&= (\delta_{ij} + \delta Z_{ij}^L) (\not{k} - m_i^{tr} - \delta m_{ij}^L + \delta Z_{ij}^L m_i^{tr}) P_L \\
&+ (\delta_{ij} + \delta Z_{ij}^R) (\not{k} - m_j^{tr} - \delta m_{ij}^R + \delta Z_{ij}^R m_j^{tr}) P_R,
\end{aligned} \tag{18}$$

where $\delta_{ij} + \delta Z_{ij}^L$ stands for the left-handed wave function's renormalization multiplier and $\delta_{ij} + \delta Z_{ij}^R$ stands for the right-handed wave function's renormalization multiplier. m_i^{tr} refers to the mass of the i th generation fermion at the tree level. Based on Eq.(18) and the mass-shell conditions, we obtain the loop corrections for the mass matrix elements as follows

$$\begin{aligned}
\delta m_{ij}^{loop} &= 3m_i^{tr} (m_i^{tr})^2 a_{ij}^1 + \left(m_i^{tr} m_j^{tr} + (m_i^{tr})^2 + (m_j^{tr})^2 \right) m_i^{tr} b_{ij}^1 \\
&+ \left((m_i^{tr})^2 m_j^{tr} + 3m_i^{tr} (m_j^{tr})^2 \right) c_{ij}^1 + \left(3(m_i^{tr})^2 m_j^{tr} + m_i^{tr} (m_i^{tr})^2 \right) d_{ij}^1.
\end{aligned} \tag{19}$$

To compute $a_{ij}^0, b_{ij}^0, c_{ij}^0, d_{ij}^0$, the one-loop self energy diagrams should be precisely calculated. The associated Feynman diagrams are shown in Fig.1. The exchanged bosons can

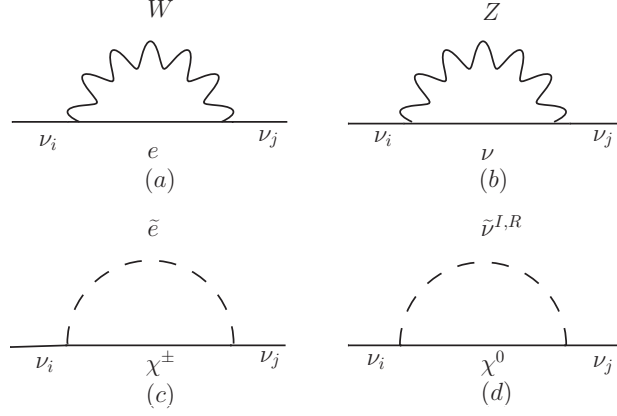


FIG. 1: The one-loop self-energy diagrams

be of vectorial or scalar type, which leads to different integral calculations. The integral for exchanging vector-boson is

$$\begin{aligned} \mathcal{M}_\nu^{a,b} &= -\bar{u}(P) \int \frac{d^D k}{(2\pi)^D} i\gamma_\mu (A_L P_L + A_R P_R) \frac{i}{\not{k} - m_F} i\gamma_\beta (B_L P_L + B_R P_R) \frac{-ig^{\alpha\beta}}{(p-k)^2 - m_V^2} u(p) \\ &= -\int_0^1 dx \int \frac{d^D k}{(2\pi)^D} \frac{1}{[k^2 - xm_V^2 - (1-x)m_F^2]} \left[1 + \frac{2x(1-x)p^2}{k^2 + xm_V^2 + (1-x)m_F^2} \right] \\ &\quad \times [A_R B_L P_L D m_F + A_L B_R P_R D m_F + A_L B_L P_L (2-D) \not{p} x + A_R B_R P_R (2-D) \not{p} x], \quad (20) \end{aligned}$$

where $D = 4 - 2\varepsilon$. m_V denotes the mass of the vector boson appearing in the loop, and m_F denotes the fermion in the loop. From Eq.(10), Eq.(11) and Eq.(20), we obtain

$$\begin{aligned} a_{ij}^0(m_V, m_F) &= iD \frac{m_F}{m_j} A_R B_L F_1(m_F, m_V), \\ b_{ij}^0(m_V, m_F) &= i \frac{m_F}{m_j} A_L B_R F_1(m_F, m_V), \\ c_{ij}^0(m_V, m_F) &= i A_L B_L F_2(m_F, m_V), \\ d_{ij}^0(m_V, m_F) &= i A_R B_R F_2(m_F, m_V), \\ a_{ij}^1(m_V, m_F) &= i \frac{m_F}{m_j} A_R B_L F_3(m_F, m_V), \\ b_{ij}^1(m_V, m_F) &= i \frac{m_F}{m_j} A_L B_R F_3(m_F, m_V), \\ c_{ij}^1(m_V, m_F) &= i A_R B_L F_4(m_F, m_V), \\ d_{ij}^1(m_V, m_F) &= i A_L B_R F_4(m_F, m_V), \end{aligned} \quad (21)$$

where F_1 , F_2 , F_3 and F_4 are integrals over the internal momentum of the loop and their explicit forms are given in appendix B. In Fig.(1)(b), the specific forms of $A_L^{Z,\nu}$, $A_R^{Z,\nu}$, $B_L^{Z,\nu}$

and $B_R^{Z,\nu}$ are

$$\begin{aligned}
A_L^{Z,\nu} &= -\frac{i}{2}(g_1 \cos \theta'_w \sin \theta_w + g_2 \cos \theta_w \cos \theta'_w) \sum_{a=1}^3 U_{j,a}^{V,*} U_{i,a}^V, \\
A_R^{Z,\nu} &= \frac{i}{2}(g_1 \cos \theta'_w \sin \theta_w + g_2 \cos \theta_w \cos \theta'_w) \sum_{a=1}^3 U_{i,a}^{V,*} U_{j,a}^V, \\
B_L^{Z,\nu} &= \frac{i}{2} \left((g_1 \sin \theta_w + g_2 \cos \theta_w) \sin \theta'_w + (g_{YB} + g_B) \cos \theta'_w \right) \sum_{a=1}^3 U_{j,a}^{V,*} U_{i,a}^V \\
&\quad - g_B \cos \theta'_w \sum_{a=1}^3 U_{j,3+a}^{V,*} U_{i,3+a}^V, \\
B_R^{Z,\nu} &= -\frac{i}{2} \left((g_1 \sin \theta_w + g_2 \cos \theta_w) \sin \theta'_w + (g_{YB} + g_B) \cos \theta'_w \right) \sum_{a=1}^3 U_{i,a}^{V,*} U_{j,a}^V \\
&\quad - g_B \cos \theta'_w \sum_{a=1}^3 U_{i,3+a}^{V,*} U_{j,3+a}^V.
\end{aligned} \tag{22}$$

θ_w denotes the Weinberg angle, and θ'_w denotes $B - L$ mixing angle. U^V denotes the rotation matrix to diagonalize the neutrino mass matrix.

For the exchange of scalar bosons, the amplitude is derived in a similar manner. And it is written as

$$\begin{aligned}
\mathcal{M}_\nu^{c,d} &= -\bar{u}(P) \int \frac{d^D k}{(2\pi)^D} i(C_L P_L + C_R P_R) \frac{i}{\not{k} - m_F} i(D_L P_L + D_R P_R) \frac{-i}{(p-k)^2 - m_S^2} u(p) \\
&= -\int_0^1 dx \int \frac{d^D k}{(2\pi)^D} \frac{1}{[k^2 - x m_S^2 - (1-x)m_F^2]} \left[1 + \frac{2x(1-x)p^2}{k^2 + x m_S^2 + (1-x)m_F^2} \right] \\
&\quad \times [(C_R D_L P_L + C_L D_R P_R) m_F + (C_L D_L P_L x + C_R D_R P_R) \not{p} x],
\end{aligned} \tag{23}$$

where m_S denotes the mass of the scalar boson appearing in the loop, and m_F denotes the fermion in the loop. From Eq.(10), Eq.(11) and Eq.(23), we obtain

$$\begin{aligned}
a_{ij}^0(m_S, m_F) &= i \frac{m_F}{m_j} C_L D_L F_1(m_F, m_S), \\
b_{ij}^0(m_S, m_F) &= i \frac{m_F}{m_j} C_R D_R F_1(m_F, m_S), \\
c_{ij}^0(m_S, m_F) &= i C_R D_L F_2(m_F, m_S), \\
d_{ij}^0(m_S, m_F) &= i C_L D_R F_2(m_F, m_S), \\
a_{ij}^1(m_S, m_F) &= i \frac{m_F}{m_j} C_L D_L F_3(m_F, m_S), \\
b_{ij}^1(m_S, m_F) &= i \frac{m_F}{m_j} C_L D_L F_3(m_F, m_S),
\end{aligned}$$

$$\begin{aligned}
c_{ij}^1(m_S, m_F) &= iC_R D_L F_4(m_F, m_S), \\
d_{ij}^1(m_S, m_F) &= iC_L D_R F_4(m_F, m_S).
\end{aligned} \tag{24}$$

In Fig.(1)(c), the specific forms of $C_L^{\chi^\pm, e, \nu}$, $C_R^{\chi^\pm, e, \nu}$, $D_L^{\chi^\pm, e, \nu}$ and $D_R^{\chi^\pm, e, \nu}$ are

$$\begin{aligned}
C_L^{\chi^\pm, e, \nu} &= -g_2 U_{j,1}^* \sum_{a=1}^3 U_{i,a}^{V,*} Z_{k,a}^E + U_{j,2} \sum_{a=1}^3 U_{i,b}^{V,*} \sum_{a=1}^3 Y_{e,ab} Z_{k,3+a}^E, \\
C_R^{\chi^\pm, e, \nu} &= \sum_{b=1}^3 \sum_{a=1}^3 Y_{\nu,ab}^* U_{i,3+a}^V Z_{k,b}^E V_{j,2}, \\
D_L^{\chi^\pm, e, \nu} &= -g_2 \sum_{a=1}^3 Z_{k,a}^{E,*} U_{j,a}^V U_{i,1} + \sum_{a=1}^3 \sum_{b=1}^3 Y_{e,ab}^* Z_{k,3+a}^{E,*} U_{j,b}^V U_{i,2}, \\
D_R^{\chi^\pm, e, \nu} &= V_{i,2}^* \sum_{b=1}^3 Z_{k,b}^{E,*} \sum_{a=1}^3 U_{j,3+a}^V Y_{\nu,ab}.
\end{aligned} \tag{25}$$

Z^E denotes the rotation matrix to diagonalize the slepton mass squared matrix. We introduce them in detail in appendix A.

At tree level, the neutrino mass mixing matrix is

$$M_\nu = \begin{pmatrix} 0 & \frac{1}{\sqrt{2}} v_u Y_\nu^T \\ \frac{1}{\sqrt{2}} v_u Y_\nu & \sqrt{2} v_\eta Y_X \end{pmatrix}. \tag{26}$$

The masses of neutrinos are obtained through the rotation matrix U^V using the formula $(U^V)^T M_\nu U^V = \text{diag}(m_{\nu\alpha})$, where $\alpha = 1 \dots 6$. Here, M_ν is the mass matrix of neutrinos, and $\text{diag}(m_{\nu\alpha})$ is the diagonalized mass matrix. We use the matrix $(U^V)^T$ in the leading order of $\zeta = \frac{v_u}{v_\eta} (Y_\nu^T)_{3 \times 3} \cdot (Y_X)^{-1}_{3 \times 3}$. Since the neutrino Yukawa coupling Y_ν is very small, all elements of ζ are much smaller than 1 ($\zeta_{IJ} \ll 1$, $I, J = 1, 2, 3$). In the leading-order approximation of ζ , $(U^V)^T$ can be expressed as

$$(U^V)^T = \begin{pmatrix} \mathcal{S}^T & 0 \\ 0 & \mathcal{R}^T \end{pmatrix} \begin{pmatrix} 1 - \frac{1}{2} \zeta^\dagger \zeta & -\zeta^\dagger \\ \zeta & 1 - \frac{1}{2} \zeta \zeta^\dagger \end{pmatrix}. \tag{27}$$

Here, \mathcal{S} and \mathcal{R} are matrices used to diagonalize M_ν^{seesaw} and $\sqrt{2} v_\eta Y_X$.

$$\begin{aligned}
\mathcal{S}^T M_\nu^{\text{seesaw}} \mathcal{S} &= \text{diag}(m_{\nu 1}, m_{\nu 2}, m_{\nu 3}), \\
\mathcal{R}^T \sqrt{2} v_\eta Y_X \mathcal{R} &= \text{diag}(m_{\nu 4}, m_{\nu 5}, m_{\nu 6}).
\end{aligned} \tag{28}$$

Here to make the discussion simple, we assume that Y_X is the diagonal matrix and $\mathcal{R} = 1$. M_ν^{seesaw} is expressed as

$$M_\nu^{\text{seesaw}} = \frac{v_u^2}{v_\eta} (Y_\nu^T)_{3 \times 3} (Y_X)^{-1}_{3 \times 3} (Y_\nu)_{3 \times 3}. \tag{29}$$

The neutrino mass mixing matrix is the sum of the tree-level result and the one-loop correction. It is expressed as follows(I, J=1, 2, 3)

$$M^{sum} = M_\nu + \delta m_{ij}^{loop} = \begin{pmatrix} m_{I,J}^{loop} & \frac{1}{\sqrt{2}}v_u Y_\nu + m_{I,J+3}^{loop} \\ \frac{1}{\sqrt{2}}v_u Y_\nu + m_{I+3,J}^{loop} & \sqrt{2}v_\eta Y_X + m_{I+3,J+3}^{loop} \end{pmatrix}. \quad (30)$$

Clearly, the matrix M^{sum} includes one-loop correction that also has a seesaw structure. At one loop level, we obtain a corrected effective light neutrino mass matrix of the form[28]

$$\begin{aligned} \mathcal{M}_\nu^{eff} \approx m_{IJ}^{loop} - & \left(\frac{1}{\sqrt{2}}v_u Y_\nu + m_{I,J+3}^{loop} \right)^T (\sqrt{2}v_\eta Y_\nu + m_{I+3,J+3}^{loop})^{-1} \\ & \times \left(\frac{1}{\sqrt{2}}v_u Y_\nu + m_{I+3,J}^{loop} \right). \end{aligned} \quad (31)$$

By the 'top-down' approach[20, 29], starting from the one-loop corrected light neutrino effective mass matrix \mathcal{M}_ν^{eff} , one can obtain the corresponding Hermitian matrix.

$$\mathcal{H} = (\mathcal{M}_\nu^{eff})^\dagger \mathcal{M}_\nu^{eff}. \quad (32)$$

By diagonalizing the 3×3 matrix \mathcal{H} , we can obtain three eigenvalues

$$\begin{aligned} m_1^2 &= \frac{a}{3} - \frac{1}{3}p(\cos \phi + \sqrt{3} \sin \phi), \\ m_2^2 &= \frac{a}{3} - \frac{1}{3}p(\cos \phi - \sqrt{3} \sin \phi), \\ m_3^2 &= \frac{a}{3} + \frac{2}{3}p \cos \phi. \end{aligned} \quad (33)$$

The specific form of the parameters in Eq.(33) is as follows

$$\begin{aligned} p &= \sqrt{a^2 - 3b}, \quad \phi = \frac{1}{3} \arccos \left(\frac{1}{p^3} \left(a^3 - \frac{9}{2}ab + \frac{27}{2}c \right) \right), \quad a = \text{Tr}(\mathcal{H}), \\ b &= \mathcal{H}_{11}\mathcal{H}_{22} + \mathcal{H}_{11}\mathcal{H}_{33} + \mathcal{H}_{22}\mathcal{H}_{33} - \mathcal{H}_{12}^2 - \mathcal{H}_{13}^2 - \mathcal{H}_{23}^2, \quad c = \text{Det}(\mathcal{H}). \end{aligned} \quad (34)$$

For the neutrino mass spectrum, there are two possibilities in the 3-neutrino mixing case. The neutrino mass spectrum with normal ordering (NO) is

$$\begin{aligned} m_{\nu 1} &< m_{\nu 2} < m_{\nu 3}, \quad m_{\nu 1}^2 = m_1^2, \quad m_{\nu 2}^2 = m_2^2, \quad m_{\nu 3}^2 = m_3^2, \\ \Delta m_\odot^2 &= m_{\nu 2}^2 - m_{\nu 1}^2 = \frac{2}{\sqrt{3}}p \sin \phi > 0, \\ \Delta m_A^2 &= m_{\nu 3}^2 - m_{\nu 2}^2 = p(\cos \phi + \frac{1}{\sqrt{3}} \sin \phi) > 0. \end{aligned} \quad (35)$$

The neutrino mass spectrum with inverse order (IO) is as follows

$$\begin{aligned}
m_{\nu 3} < m_{\nu 1} < m_{\nu 2}, \quad m_{\nu 3}^2 &= m_1^2, \quad m_{\nu 1}^2 = m_2^2, \quad m_{\nu 2}^2 = m_3^2, \\
\Delta m_{\odot}^2 &= m_{\nu 2}^2 - m_{\nu 1}^2 = p(\cos \phi - \frac{1}{\sqrt{3}} \sin \phi) > 0, \\
\Delta m_A^2 &= m_{\nu 3}^2 - m_{\nu 2}^2 = -p(\cos \phi + \frac{1}{\sqrt{3}} \sin \phi) < 0.
\end{aligned} \tag{36}$$

The specific forms of the three mixing angles are shown in the Appendix C.

IV. NUMERICAL ANALYSIS

In this section, we discuss the numerical results of neutrino masses and mixing angles. We use the parameter space of the N-B-LSSM and focus on the small neutrino Yukawa couplings. These couplings can contribute to the masses of light neutrinos at the tree level through the first type seesaw mechanism. The neutrino Yukawa coupling matrix Y_ν is a key parameter. It affects the masses of light neutrinos. Since the masses of light neutrinos are very small, we need to carefully consider and precisely calculate it. Therefore, the parameters used must be highly accurate. When performing the calculations, the following experimental limitations need to be taken into account:

1. We consider that the experimental constraint from the lightest CP-even Higgs mass is 125.20 ± 0.11 GeV[30–32].
2. The Z' boson mass is larger than 5.1 TeV. The ratio between $M_{Z'}$ and its gauge $M_{Z'}/g_B \geq 6$ TeV[33].
3. The new angle β_η is constrained by LHC as $\tan \beta_\eta < 1.5$.
4. The limitations for the particle masses are the following[34–39]. The neutralino mass is limited to more than 116 GeV, the chargino mass is limited to more than 1100 GeV and the slepton mass is greater than 700 GeV. Considering these limitations, we adopt the following parameters

$$\begin{aligned}
\tan \beta &= 15, \quad \tan \beta_\eta = 0.62, \quad g_B = 0.27, \quad g_{YB} = -0.18, \\
\lambda_2 &= -0.25, \quad \lambda = 0.3, \quad M_1 = 800 \text{ GeV}, \quad M_2 = 1100 \text{ GeV}, \\
v_S &= 5 \text{ TeV}, \quad \kappa = 0.04, \quad M_{BL} = 1000 \text{ GeV}, \quad M_{BB'} = 1100 \text{ GeV}, \\
v_\eta &= 37.6 * \cos \theta_\eta \text{ TeV}, \quad v_{\bar{\eta}} = 37.6 * \sin \theta_\eta \text{ TeV}, \quad \tan \theta_\eta = 0.62, \\
m_{\tilde{L}ii}^2 &= 1073^2 \text{ GeV}^2, \quad m_{\tilde{\nu}ii}^2 = 1 \times 10^6 \text{ GeV}^2, \quad T_{Xii} = -4000 \text{ GeV},
\end{aligned}$$

TABLE II: Current experimental uncertainties and future sensitivities[40–42].

| parameters | Ordering | PDG2024 | $1\sigma(\%)$ | Prospect(%, years) |
|--|----------|---------------------------|---------------|--------------------|
| $\frac{\Delta m_{21}^2}{10^{-5}\text{eV}^2}$ | NO, IO | 7.53 ± 0.18 | 2.4 | (0.3, 6) |
| $\frac{ \Delta m_{32}^2 }{10^{-3}\text{eV}^2}$ | NO | 2.455 ± 0.028 | 1.1 | (0.2, 6) |
| | IO | 2.529 ± 0.029 | 1.1 | |
| $\sin^2 \theta_{12}$ | NO, IO | 0.307 ± 0.013 | 4.2 | (0.5, 6) |
| $\frac{\sin^2 \theta_{13}}{10^{-2}}$ | NO, IO | 2.19 ± 0.07 | 3.2 | (2.9, -) |
| $\sin^2 \theta_{23}$ | NO | $0.558^{+0.015}_{-0.024}$ | 3.6 | (0.7-3.4, 10) |
| | IO | $0.553^{+0.016}_{-0.024}$ | 3.7 | |

$$\begin{aligned}
 T_{\nu ii} &= 1000 \text{ GeV}, \quad T_{eii} = 1000 \text{ GeV}, \quad Y_{Xii} = 0.43, \\
 m_{Eii}^2 &= 1.7 \times 10^6 \text{ GeV}^2 \quad (i = 1, 2, 3).
 \end{aligned} \tag{37}$$

In this study, the numerical results imply that the one-loop corrections contribute approximately 10% to the total results including tree and one-loop contributions. Here we show the current experimental uncertainty and the future sensitivity in the table II[40–42], where we can find the current experimental uncertainties of neutrino mass squared difference and mixing angles vary from 1.1% to 4.2%. The corresponding future sensitivities are proposed in the approximated region [0.2%, 3.4%]. In the end, one can find that the one-loop corrections are about 3 ∼ 5 times as the current experiment sensitivities. Therefore, it is important to consider the one loop corrections to the neutrino mass and mixing.

The main effect is due to the tree-level seesaw contribution. We want to obtain an approximate analytic understanding of the result at tree level. It would be good to explain the numerical results using analytic estimates. So, we perform approximate analytic analysis at normal order and inverse order.

A. Approximate analysis of the mass matrix at tree level (NO)

At first, we discuss the approximate analytic understanding for the NO condition. Without any setting and approximation, the analytic results will be very complicated and impossible to read. Therefore, we use the following relations to simplify the discussion

$$(Y_\nu)^{11} = -1.8 \times (Y_\nu)^{22}, \quad (Y_\nu)^{23} = 2.6 \times (Y_\nu)^{22}, \quad (Y_\nu)^{12} = (Y_\nu)^{13} = 1.5 \times (Y_\nu)^{33}. \tag{38}$$

Then the remaining two variables of the Yukawa coupling elements $(Y_\nu)^{ij}$ with $i, j = 1, 2, 3$ are $(Y_\nu)^{22}$ and $(Y_\nu)^{33}$. With the values for v_u, v_η, Y_X in Eq.(37), when we adjust the values of the both variables $(Y_\nu)^{22}$ and $(Y_\nu)^{33}$, ϕ is a small value, stable around 0.0267. So, we simplify the formulas for neutrino mass in Eqs.(33)(35) with the assumption $\sin \phi \sim \phi \sim 0.0267$ and $\cos \phi \sim 1$,

$$\begin{aligned}
m_1^2 &= \frac{a}{3} - \frac{1}{3}p(1 + \sqrt{3} * 0.0267), \\
m_2^2 &= \frac{a}{3} - \frac{1}{3}p(1 - \sqrt{3} * 0.0267), \\
m_3^2 &= \frac{a}{3} + \frac{2}{3}p, \\
\Delta m_\odot^2 &= m_{\nu_2}^2 - m_{\nu_1}^2 = \frac{2}{\sqrt{3}}p * 0.0267, \\
\Delta m_A^2 &= m_{\nu_3}^2 - m_{\nu_1}^2 = p(1 + \frac{1}{\sqrt{3}} * 0.0267).
\end{aligned} \tag{39}$$

In this condition, a and p are

$$\begin{aligned}
a &= \frac{1}{2v_\eta^2 Y_X^2} (-129.933\epsilon_{22}^4 - 27.04\epsilon_{22}^3\epsilon_{33} - 162.4\epsilon_{22}^2\epsilon_{33}^2 - 30.6\epsilon_{22}\epsilon_{33}^3 - 50.5\epsilon_{33}^4), \\
p &= \frac{1}{2v_\eta^2 Y_X^2} \left(6856.37\epsilon_{22}^8 + 9882.19\epsilon_{22}^7\epsilon_{33} + 22477.8\epsilon_{22}^6\epsilon_{33}^2 + 20979.9\epsilon_{22}^5\epsilon_{33}^3 \right. \\
&\quad \left. + 22631.7\epsilon_{22}^4\epsilon_{33}^4 + 13669.1\epsilon_{22}^3\epsilon_{33}^5 + 8704.7\epsilon_{22}^2\epsilon_{33}^6 + 2811.15\epsilon_{22}\epsilon_{33}^7 + 1016.31\epsilon_{33}^8 \right)^{1/2}, \tag{40}
\end{aligned}$$

with $\epsilon_{ij} = \frac{v_u}{\sqrt{2}}(Y_\nu)^{ij}$ and $Y_{X11} \simeq Y_{X22} \simeq Y_{X33} \simeq Y_X$.

As $(Y_\nu)^{22} = 1.4 \times 10^{-6}$ and $(Y_\nu)^{33} = 5.0 \times 10^{-7}$, the approximate numerical results are

$$\begin{aligned}
m_{\nu_1} &\simeq 1.743 \times 10^{-2} \text{ eV}, \quad m_{\nu_2} \simeq 1.997 \times 10^{-2} \text{ eV}, \quad m_{\nu_3} \simeq 5.863 \times 10^{-2} \text{ eV}, \\
\Delta m_\odot^2 &= 9.513 \times 10^{-5} \text{ eV}^2, \quad \Delta m_A^2 = 3.133 \times 10^{-3} \text{ eV}^2.
\end{aligned} \tag{41}$$

B. Approximate analysis of the mass matrix at tree level (IO)

In the similar way, we study the tree level neutrino mass in the IO condition with following relations

$$\begin{aligned}
(Y_\nu)^{12} &= -2.0 \times (Y_\nu)^{22}, \quad (Y_\nu)^{11} = 1.4 \times (Y_\nu)^{22}, \\
(Y_\nu)^{33} &= -0.2 \times (Y_\nu)^{23}, \quad (Y_\nu)^{13} = 1.5 \times (Y_\nu)^{23}.
\end{aligned} \tag{42}$$

The remaining variables are $(Y_\nu)^{22}$ and $(Y_\nu)^{23}$, with the simplified results of a and p

$$a = \frac{1}{2v_\eta^2 Y_X^2} (-106.602\epsilon_{22}^4 - 16.04\epsilon_{22}^2\epsilon_{23}^2 - 1.48\epsilon_{22}\epsilon_{23}^3 - 21.6466\epsilon_{23}^4), \quad (43)$$

$$p = \frac{1}{2v_\eta^2 Y_X^2} \left(11226.8\epsilon_{22}^8 + 855.576\epsilon_{22}^6\epsilon_{23}^2 - 314.412\epsilon_{22}^5\epsilon_{23}^3 - 1578.84\epsilon_{22}^4\epsilon_{23}^4 \right. \\ \left. - 63.6909\epsilon_{22}^3\epsilon_{23}^5 + 314.746\epsilon_{22}^2\epsilon_{23}^6 + 110.971\epsilon_{22}\epsilon_{23}^7 + 133.876\epsilon_{23}^8 \right)^{1/2}. \quad (44)$$

In this condition, ϕ is very near $\frac{\pi}{3}$ with the remaining two variables $(Y_\nu)^{22}$ and $(Y_\nu)^{23}$. To deal with Δm_\odot^2 better, we adopt $\phi = \frac{\pi}{3} - \delta\phi$, and obtain the following approximate results keeping the first order of $\delta\phi$.

$$\begin{aligned} m_1^2 &= \frac{a}{3} - \frac{2}{3}p, \\ m_2^2 &= \frac{a}{3} - \frac{1}{3}p(-1 + \sqrt{3}\delta\phi), \\ m_3^2 &= \frac{a}{3} + \frac{2}{3}p\left(\frac{1}{2} + \frac{\sqrt{3}}{2}\delta\phi\right), \\ \Delta m_\odot^2 &= m_{\nu_2}^2 - m_{\nu_1}^2 = p\frac{2\delta\phi}{\sqrt{3}}, \\ \Delta m_A^2 &= m_{\nu_3}^2 - m_{\nu_2}^2 = -p\left(1 + \frac{1}{\sqrt{3}}\delta\phi\right). \end{aligned} \quad (45)$$

Here, we use $(Y_\nu)^{22} = 1.4 \times 10^{-6}$ and $(Y_\nu)^{23} = 2.302 \times 10^{-6}$, then $\delta\phi$ is around 0.024. The numerical results read as

$$\begin{aligned} m_{\nu_1} &\simeq 6.139 \times 10^{-2} \text{ eV}, \quad m_{\nu_2} \simeq 6.147 \times 10^{-2} \text{ eV}, \quad m_{\nu_3} \simeq 2.169 \times 10^{-2} \text{ eV}, \\ \Delta m_\odot^2 &= 9.154 \times 10^{-5} \text{ eV}^2, \quad \Delta m_A^2 = 3.348 \times 10^{-3} \text{ eV}^2. \end{aligned} \quad (46)$$

C. NO spectrum numerical analysis

To simplify the calculations, we have assumed that the Yukawa coupling matrix is a symmetric matrix ($Y_\nu = Y_\nu^T$). This assumption reduces the number of independent parameters from 9 to 6. We further assume that Y_ν is a real matrix. The both assumptions do not affect the calculation substantively, which simplifies the computation.

Firstly, we study the neutrino mass spectrum at normal mass order (NO) by adjusting the model parameters. When the neutrino Yukawa coupling parameters are

$$(Y_\nu)^{11} = -2.5143 \times 10^{-6}, \quad (Y_\nu)^{22} = 1.4 \times 10^{-6},$$

$$\begin{aligned}
(Y_\nu)^{33} &= 5.1348 \times 10^{-7}, & (Y_\nu)^{12} &= 7.6533 \times 10^{-7}, \\
(Y_\nu)^{13} &= 7.9732 \times 10^{-7}, & (Y_\nu)^{23} &= 3.6832 \times 10^{-6}.
\end{aligned} \tag{47}$$

The following values for the neutrino mass variances and mixing angles are obtained

$$\begin{aligned}
\Delta m_A^2 &= 2.47 \times 10^{-3} \text{ eV}^2, & \Delta m_\odot^2 &= 7.89 \times 10^{-5} \text{ eV}^2, \\
m_{\nu_1} &= 1.52 \times 10^{-2} \text{ eV}, & m_{\nu_2} &= 1.76 \times 10^{-2} \text{ eV}, & m_{\nu_3} &= 5.20 \times 10^{-2} \text{ eV}, \\
\sin^2 \theta_{13} &= 0.0225, & \sin^2 \theta_{12} &= 0.268, & \sin^2 \theta_{23} &= 0.562.
\end{aligned} \tag{48}$$

We scan pure loop-level parameters such as g_{YB} , whose influence to the one-loop corrections is approximately at the 10% level. One-loop corrections account for approximately 10% of the tree level results. Therefore, in the summary, the impact of g_{YB} is estimated to be around 1% of the total results. Due to this relatively minor variation, it's hard to see the change of the result in the graph. So, near the 3σ region of neutrino experiment data, we choose the other parameters as variables to plot figures in the following.

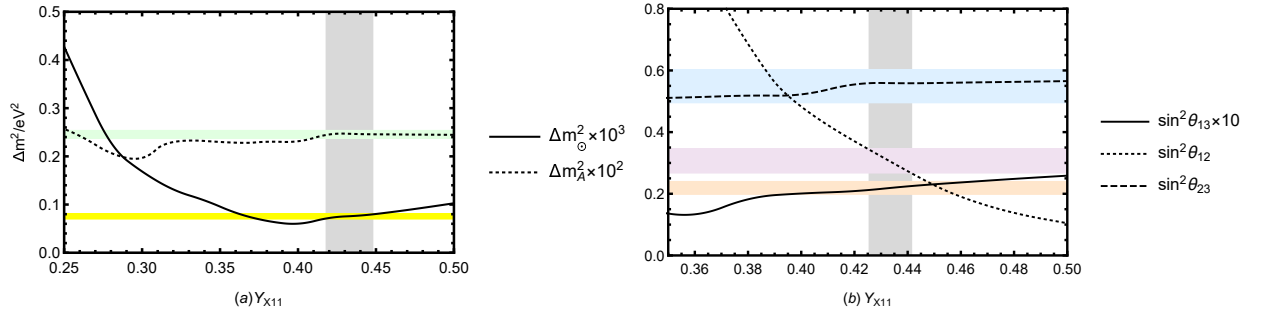


FIG. 2: The neutrino mass-squared differences and mixing angles versus Y_{X11} . The coloured bands in the figure represent experimental limits in the range of 3σ .

Y_X directly generates the right-handed neutrino mass term and indirectly modulates loop corrections to the neutrino mass matrix. Fig.2 examines the impact of Y_{X11} on neutrino mass-squared differences and mixing angles. Fig.2(a) displays the evolution of Δm_A^2 and Δm_\odot^2 across $Y_{X11} \in [0.25, 0.5]$. The mass-squared difference Δm_A^2 tends to change steadily after slowly decrease. In contrast, Δm_\odot^2 exhibits a clear decline trend then tends to be stable. Both Δm_\odot^2 and Δm_A^2 converge within experimental constraints (gray band) for $Y_{X11} \in [0.419, 0.45]$. Fig.2(b) displays the Y_{X11} effects (0.35 to 0.5) on mixing angles $\sin^2 \theta_{12}$, $\sin^2 \theta_{13}$, and $\sin^2 \theta_{23}$. Both $\sin^2 \theta_{13}$ and $\sin^2 \theta_{23}$ demonstrate a gradual increasing trend. Conversely, $\sin^2 \theta_{12}$ decreases clearly with increasing Y_{X11} . Crucially, all mixing angles simultaneously

satisfy experimental limits within $Y_{X11} \in [0.425, 0.442]$ (gray region). To ensure consistency with other parameters, we take $Y_{X11} = 0.43$ as the benchmark value.

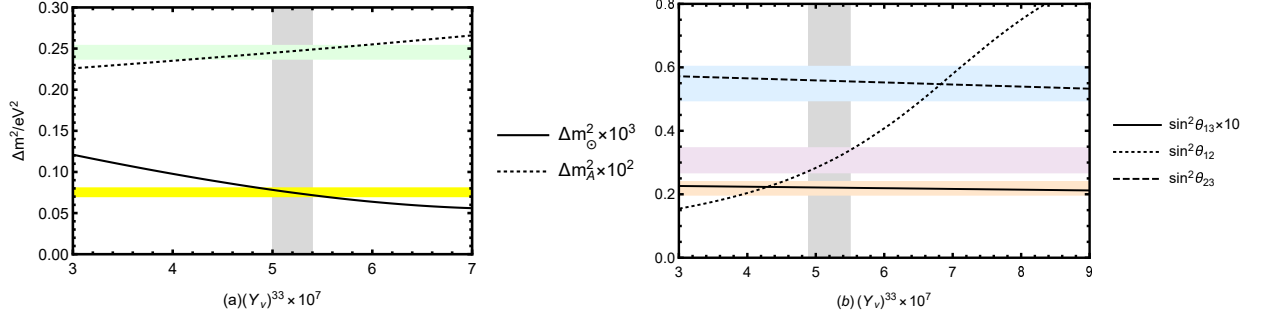


FIG. 3: The neutrino mass-squared differences and mixing angles versus $(Y_\nu)^{33}$. The coloured bands in the figure represent experimental limits in the range of 3σ .

Despite the fact that neutrino Yukawa couplings coefficient are very small, they have a very significant effect on the neutrino mass and mixing angle, mainly due to their contribution at the tree level. Fig. 3(a) shows the evolution of the mass-squared differences (Δm_A^2 and Δm_\odot^2) across a scan of $(Y_\nu)^{33}$ from 3×10^{-7} to 7×10^{-7} . Over this domain, Δm_A^2 undergoes a slight rise. Conversely, Δm_\odot^2 shows a significant decrease. Crucially, both fall within experimentally allowed ranges (gray band) for $(Y_\nu)^{33}$ values between 5×10^{-7} and 5.4×10^{-7} . The corresponding variations in the neutrino mixing angles are plotted in Fig.3(b). $\sin^2 \theta_{13}$ decreases with increasing $(Y_\nu)^{33}$, though the magnitude of change is marginal. $\sin^2 \theta_{23}$ is also decreasing but the variation is slightly larger than that of $\sin^2 \theta_{13}$. In contrast, $\sin^2 \theta_{12}$ experiences a consistent upward change. At the benchmark point $(Y_\nu)^{33} = 5.1348 \times 10^{-7}$, all neutrino mass-squared differences and mixing angles concurrently align with established experimental limits.

In addition to the diagonal factors, the non-diagonal elements of Y_ν are also very important in our discussion. We investigate the impact of $(Y_\nu)^{13}$ on theoretical predictions for neutrino mass-squared differences and mixing angles in Fig.4. Fig.4(a) displays the evolution of Δm_A^2 and Δm_\odot^2 with varying $(Y_\nu)^{13}$. The mass-squared difference Δm_A^2 exhibits a stable, near-linear rise across the parameter range. Conversely, Δm_\odot^2 demonstrates a two-phase evolution: first showing a slight decrease followed by a significant upward trend. Both quantities converge within experimental bounds (gray band) in the vicinity of $(Y_\nu)^{13} = 7.9732 \times 10^{-7}$. The corresponding mixing angle variations are shown in Fig.4(b). $\sin^2 \theta_{13}$ exhibits a grad-

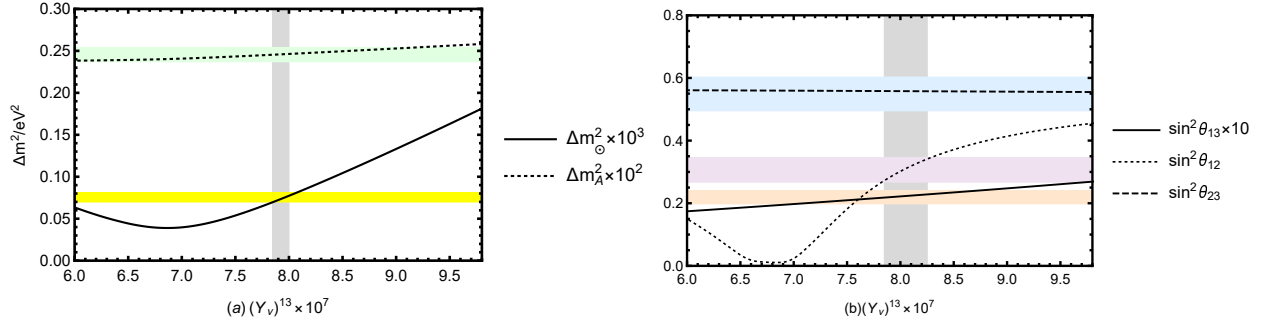


FIG. 4: The neutrino mass-squared differences and mixing angles versus $(Y_\nu)^{13}$. The coloured bands in the figure represent experimental limits in the range of 3σ .

ual increase and $\sin^2 \theta_{23}$ exhibits fairly stable over the scanned range. In contrast, $\sin^2 \theta_{12}$ undergoes a different characteristic: decreasing initially before trending upward at around $(Y_\nu)^{13} = 6.8 \times 10^{-7}$. Remarkably, at the benchmark value $(Y_\nu)^{13} = 7.9732 \times 10^{-7}$, the theoretical predictions for mass-squared differences and mixing angles simultaneously satisfy the experimental constraints.

D. IO spectrum numerical analysis

If the neutrino mass spectrum is IO, we use the following Yukawa coupling parameters

$$\begin{aligned}
 (Y_\nu)^{11} &= 1.89623 \times 10^{-6}, & (Y_\nu)^{22} &= 1.4 \times 10^{-6}, \\
 (Y_\nu)^{33} &= -4.38536 \times 10^{-7}, & (Y_\nu)^{12} &= -2.87584 \times 10^{-6}, \\
 (Y_\nu)^{13} &= 3.42168 \times 10^{-6}, & (Y_\nu)^{23} &= 2.30264 \times 10^{-6}.
 \end{aligned} \tag{49}$$

Numerical results are obtained for the neutrino mass variance and mixing angle. The numerical results are as follows

$$\begin{aligned}
 |\Delta m_A^2| &= 2.53 \times 10^{-3} \text{ eV}^2, & \Delta m_\odot^2 &= 7.605 \times 10^{-5} \text{ eV}^2, \\
 m_{\nu_1} &= 5.29 \times 10^{-2} \text{ eV}, & m_{\nu_2} &= 5.36 \times 10^{-2} \text{ eV}, & m_{\nu_3} &= 1.86 \times 10^{-2} \text{ eV}, \\
 \sin^2 \theta_{13} &= 0.0219, & \sin^2 \theta_{12} &= 0.311, & \sin^2 \theta_{23} &= 0.552.
 \end{aligned} \tag{50}$$

Fig.5(a) exhibits the effect of Y_{X11} on the mass variances Δm_A^2 and Δm_\odot^2 , and the right panel shows the effect of Y_{X11} on the three mixing angles $\sin^2 \theta_{12}$, $\sin^2 \theta_{13}$, and $\sin^2 \theta_{23}$. In

Fig.5(b), the trend of Δm_{\odot}^2 is shown to be relatively stable, and small changes in Y_{X11} in the range $0.43 - 0.443$ have a significant effect on Δm_A^2 . In Fig.5(b), it is shown that the value of $\sin^2 \theta_{23}$ remains stable in the Y_{X11} range $0.43 - 0.443$. $\sin^2 \theta_{13}$ overall decreases slightly and then tends to stabilise. $\sin^2 \theta_{12}$ decreases rapidly and then increases slowly in a wave-like manner. All three mixing angles near $Y_{X11}=0.434$ conform to the experimental limits.

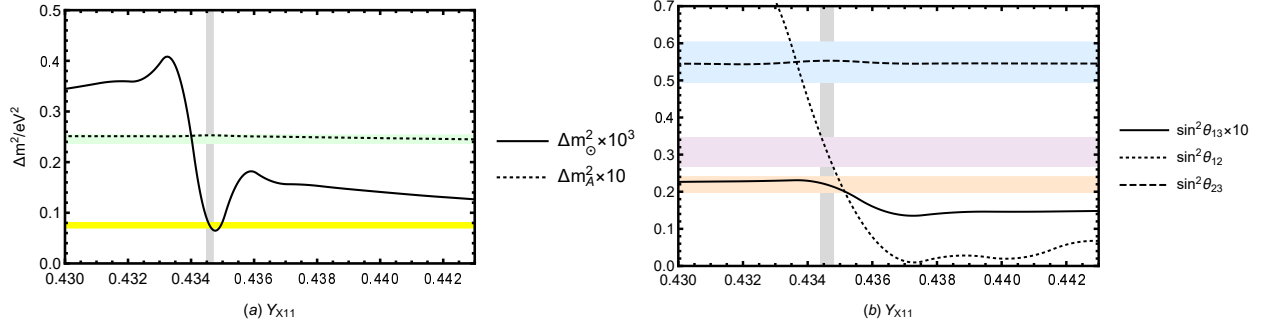


FIG. 5: The neutrino mass-squared differences and mixing angles versus Y_{X11} . The coloured bands in the figure represent experimental limits in the range of 3σ .

Here we discuss the effect of the diagonal elements of Y_{ν} . Fig.6 shows the effect of $(Y_{\nu})^{33}$ on the neutrino mass variances and the three mixing angles. When $(Y_{\nu})^{33}$ is in the range of $-4.45 \times 10^{-7} - -4.38 \times 10^{-7}$, as a whole, the five values change relatively smoothly. When $(Y_{\nu})^{33}$ is in the range of $-4.45 \times 10^{-7} - -4.38 \times 10^{-7}$ all five values are in accordance with the experimental limits (i.e. left side of the red line). On the right side of the red line in Fig.6(a), Δm_A^2 stably decreases and Δm_{\odot}^2 shows an increasing trend. On the right side of the red line in Fig.6(b), $\sin^2 \theta_{23}$ changes more smoothly, $\sin^2 \theta_{12}$ decreases and then increases, and $\sin^2 \theta_{13}$ vice versa.

We also discuss how the non-diagonal element $(Y_{\nu})^{13}$ affects the theoretical predictions of the neutrino mixing angle and the mass-squared difference in Fig.7. As can be seen in the Fig.7(a), the change in Δm_{\odot}^2 is smoother and $(Y_{\nu})^{13}$ has a significant effect on Δm_A^2 . Both reach the experimental limit near 3.42×10^{-6} . The Fig.7(b) shows the effect of $(Y_{\nu})^{13}$ on the three mixing angles. $\sin^2 \theta_{13}$ shows a smooth decline followed by a rise. $\sin^2 \theta_{23}$ rises slowly. $\sin^2 \theta_{12}$ is more stable in the range of $3.35 \times 10^{-6} - 3.50 \times 10^{-6}$, followed by a declining trend. To harmonise the other parameters, $(Y_{\nu})^{13}$ takes the value of 3.42168×10^{-6} .

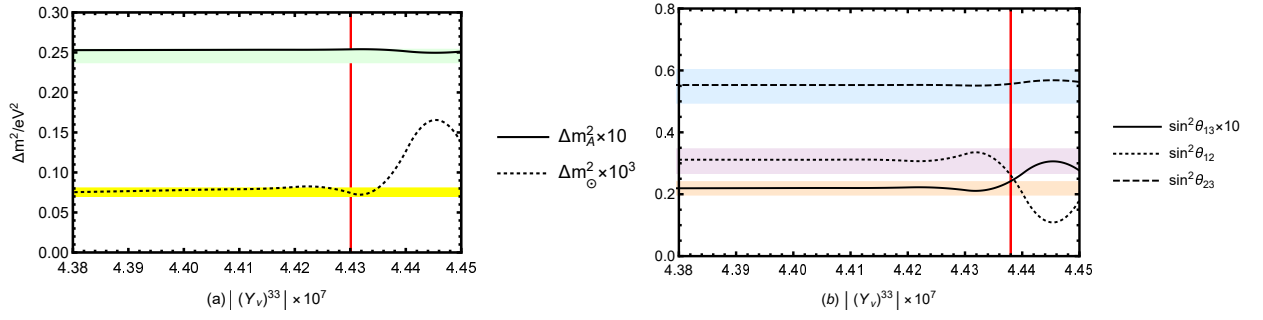


FIG. 6: The neutrino mass-squared differences and mixing angles versus $(Y_\nu)^{33}$. The coloured bands in the figure represent experimental limits in the range of 3σ .

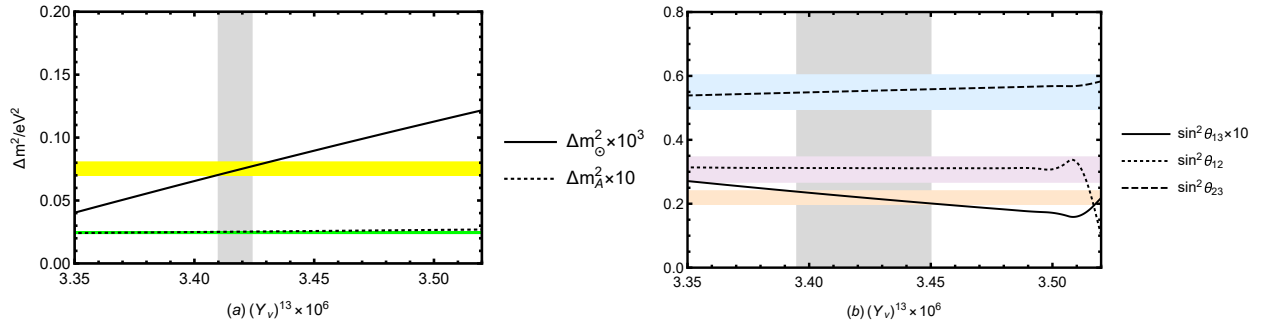


FIG. 7: The neutrino mass squared differences and mixing angles versus $(Y_\nu)^{13}$. The coloured bands in the figure represent experimental limits in the range of 3σ .

V. CONCLUSION

The SM cannot resolve the neutrino mass problem, and physicists believe that the SM should be a low-energy effective theory of large model. Therefore, the SM should be extended. The N-B-LSSM is a symmetry extension of the MSSM, in which we have investigated some processes in our previous work. The one-loop corrections to the neutrino mixing matrix are studied in this work.

In this paper, we systematically study the one-loop correction to the neutrino mass matrix in the N-B-LSSM and its fitting to experimental data on neutrino oscillations. We analyse the contributions to the neutrino mass from the loop diagrams of scalar lepton-chargino, scalar neutrino-neutralino and so on. Then we obtain the sum of tree-level and one-loop contributions to the neutrino mixing matrix. The one-loop corrected light neutrino effective mass matrix M_ν^{eff} is derived, and using the 'top-down' approach, we give formulas for the

neutrino mass variances and mixing angles. For the neutrino mass spectra, NO and IO conditions are discussed numerically. The light neutrino masses are very tiny and there are five experiment constraints (three mixing angles and two mass squared differences), the obtained suitable parameter space is narrow. The numerical results show that the model can fit the current experimental data, including the neutrino mass squared deviation and the mixing angle, well within a specific parameter range.

Appendix A: Mass matrix and coupling in N-B-LSSM

The mass matrix for chargino is

$$m_{\chi^\pm} = \begin{pmatrix} M_2 & \frac{1}{\sqrt{2}}g_2v_\mu \\ \frac{1}{\sqrt{2}}g_2v_d & \frac{1}{\sqrt{2}}\lambda v_S \end{pmatrix}. \quad (\text{A1})$$

This matrix is diagonalized by U and V

$$U^* m_{\chi^\pm} V^\dagger = m_{\chi^\pm}^{dia}. \quad (\text{A2})$$

The mass matrix for slepton is

$$m_{\tilde{e}}^2 = \begin{pmatrix} m_{\tilde{e}_L\tilde{e}_L^*} & \frac{1}{\sqrt{2}}v_d T_e^\dagger - \frac{1}{2}v_u \lambda v_S Y_e^\dagger \\ \frac{1}{\sqrt{2}}v_d T_e - \frac{1}{2}v_u \lambda^* v_S Y_e & m_{\tilde{e}_R\tilde{e}_R^*} \end{pmatrix}, \quad (\text{A3})$$

$$\begin{aligned} m_{\tilde{e}_L\tilde{e}_L^*} &= m_{\tilde{L}}^2 + \frac{1}{8} \left((g_1^2 + g_{YB}^2 + g_{YB}g_B - g_2^2)(v_d^2 - v_u^2) + 2(g_B^2 + g_{YB}g_B)(v_\eta^2 - v_{\bar{\eta}}^2) \right) + \frac{v_d^2}{2}Y_e^2, \\ m_{\tilde{e}_R\tilde{e}_R^*} &= m_{\tilde{E}}^2 - \frac{1}{8} \left([2(g_1^2 + g_{YB}^2) + g_{YB}g_B](v_d^2 - v_u^2) \right. \\ &\quad \left. + (4g_{YB}g_B + 2g_B^2)(v_\eta^2 - v_{\bar{\eta}}^2) \right) + \frac{1}{2}v_d^2 Y_e^2. \end{aligned} \quad (\text{A4})$$

The matrix is diagonalized by Z^E

$$Z^E m_{\tilde{e}}^2 Z^{E,\dagger} = m_{2,\tilde{e}}^{diag}. \quad (\text{A5})$$

The mass matrix for CP-odd sneutrino is

$$m_{\nu^I}^2 = \begin{pmatrix} m_{\sigma_L\sigma_L} & m_{\sigma_R\sigma_L} \\ m_{\sigma_L\sigma_R} & m_{\sigma_R\sigma_R} \end{pmatrix}, \quad (\text{A6})$$

$$\begin{aligned}
m_{\sigma_L \sigma_L} &= +\frac{1}{8} \mathbf{1} \left(2g_B^2(-v_\eta^2 + v_\eta^2) + (g_1^2 + g_{YB}^2 + g_2^2)(-v_u^2 + v_d^2) \right. \\
&\quad \left. + g_{YB}g_B(-2v_\eta^2 + 2v_\eta^2 - v_\eta^2 + v_\eta^2) \right) + \frac{1}{4} \left(2v_u^2 \Re(Y_\nu^T Y_\nu^*) + 4\Re(m_L^2) \right), \\
m_{\sigma_L \sigma_R} &= \frac{1}{4} \left(-2v_d v_S \Re(Y_\nu \lambda^*) + 2v_u [-2v_\eta \Re(Y_X Y_\nu^*) + \sqrt{\Re(T_\nu)}] \right), \\
m_{\sigma_R \sigma_R} &= +\frac{1}{8} \mathbf{1} \left(-2g_B^2(-v_\eta^2 + v_\eta^2) + g_{YB}g_B(-v_d^2 + v_\eta^2) \right) \\
&\quad + \frac{1}{4} \left(2[2\Re(m_\nu^2) + 2v_S v_\eta \Re(Y_X \lambda_2^*)] + 2v_u^2 \Re(Y_\nu Y_\nu^\dagger) - 4\sqrt{2}v_\eta \Re(T_X) + 8v_\eta^2 \Re(Y_X Y_X^*) \right) \quad (A7)
\end{aligned}$$

This matrix is diagonalized by Z^I

$$Z^I m_{\nu^I}^2 Z^{I,\dagger} = m_{2,\nu^I}^{dia}, \quad (A8)$$

The mass matrix for CP-even sneutrino is

$$m_{\nu^R}^2 = \begin{pmatrix} m_{\phi_L \phi_L} & m_{\phi_R \phi_L}^T \\ m_{\phi_L \phi_R} & m_{\phi_R \phi_R} \end{pmatrix}, \quad (A9)$$

$$\begin{aligned}
m_{\phi_L \phi_L} &= +\frac{1}{8} \mathbf{1} \left(2g_B^2(-v_\eta^2 + v_\eta^2) + (g_1^2 + g_{YB}^2 + g_2^2)(-v_u^2 + v_d^2) \right. \\
&\quad \left. + g_{YB}g_B(-2v_\eta^2 + 2v_\eta^2 - v_\eta^2 + v_\eta^2) \right) + \frac{1}{4} \left(2v_u^2 \Re(Y_\nu^T Y_\nu^*) + 4\Re(m_L^2) \right), \\
m_{\phi_L \phi_R} &= \frac{1}{4} \left(-2v_d v_S \Re(Y_\nu \lambda^*) + 2v_u [2v_\eta \Re(Y_X Y_\nu^*) + \sqrt{\Re(T_\nu)}] \right), \\
m_{\phi_R \phi_R} &= +\frac{1}{8} \mathbf{1} \left(-2g_B^2(-v_\eta^2 + v_\eta^2) + g_{YB}g_B(-v_d^2 + v_\eta^2) \right) \\
&\quad + \frac{1}{4} \left(2v_u^2 \Re(Y_\nu Y_\nu^\dagger) + 4\Re(m_\nu^2) + 4\Re(m_\nu^2) \right. \\
&\quad \left. + 4v_\eta [2v_\eta \Re(Y_X Y_X^*) + \sqrt{2}\Re(T_X)] - 4v_S v_\eta \Re(Y_X \lambda_2^*) \right). \quad (A10)
\end{aligned}$$

This matrix is diagonalized by Z^R

$$Z^R m_{\nu^R}^2 Z^{R,\dagger} = m_{2,\nu^R}^{dia}. \quad (A11)$$

Appendix B: The definition of F_1, F_2, F_3, F_4

$$\begin{aligned}
F_1(m_1, m_2) &= \frac{1}{16\pi^2} \left(1 + \frac{1}{(m_1^2 - m_2^2)} \left(m_1^2 \log \frac{4\pi\mu^2}{m_1^2} - m_2^2 \log \frac{4\pi\mu^2}{m_2^2} \right) \right), \\
F_2(m_1, m_2) &= \frac{1}{64\pi^2} \left(-\frac{m_1^2 - 3m_2^2}{2m_1^2 - 2m_2^2} + \frac{(m_1^4 - 2m_1^2 m_2^2) \log m_1^2}{(m_1^2 - m_2^2)^2} \right)
\end{aligned}$$

$$\begin{aligned}
& + \frac{m_2^4 \log m_2^2}{(m_1^2 - m_2^2)^2} + \log 4\pi\mu^2 \Big), \\
F_3(m_1, m_2) &= \frac{1}{32(m_1^2 - m_2^2)^3 \pi^2} \left(m_1^4 - m_2^4 - 2m_1^2 m_2^2 \log \frac{m_1^2}{m_2^2} \right), \\
F_4(m_1, m_2) &= \frac{1}{96(m_1^2 - m_2^2)^4 \pi^2} (m_1^6 - 6m_1^4 m_2^2 + 3m_1^2 m_2^4 + 2m_2^6 + 6m_1^2 m_2^4 \log \frac{m_1^2}{m_2^2}). \quad (\text{B1})
\end{aligned}$$

Appendix C: Specific forms of the three mixing angles

The mass-squared matrix \mathcal{H} can be obtained to get the normalised eigenvectors as follows

$$\begin{aligned}
\begin{pmatrix} (U_\nu)_{11} \\ (U_\nu)_{21} \\ (U_\nu)_{31} \end{pmatrix} &= \frac{1}{\sqrt{|X_1|^2 + |Y_1|^2 + |Z_1|^2}} \begin{pmatrix} X_1 \\ Y_1 \\ Z_1 \end{pmatrix}, \\
\begin{pmatrix} (U_\nu)_{12} \\ (U_\nu)_{22} \\ (U_\nu)_{32} \end{pmatrix} &= \frac{1}{\sqrt{|X_2|^2 + |Y_2|^2 + |Z_2|^2}} \begin{pmatrix} X_2 \\ Y_2 \\ Z_2 \end{pmatrix}, \\
\begin{pmatrix} (U_\nu)_{13} \\ (U_\nu)_{23} \\ (U_\nu)_{33} \end{pmatrix} &= \frac{1}{\sqrt{|X_3|^2 + |Y_3|^2 + |Z_3|^2}} \begin{pmatrix} X_3 \\ Y_3 \\ Z_3 \end{pmatrix}. \quad (\text{C1})
\end{aligned}$$

The specific forms of X_I, Y_I, Z_I when $I = 1, 2, 3$ are as follows

$$\begin{aligned}
X_1 &= (\mathcal{H}_{22} - m_{\nu 1}^2)(\mathcal{H}_{33} - m_{\nu 1}^2) - \mathcal{H}_{23}^2, & Y_1 &= \mathcal{H}_{13}\mathcal{H}_{23} - \mathcal{H}_{12}(\mathcal{H}_{33} - m_{\nu 1}^2), \\
Z_1 &= \mathcal{H}_{12}\mathcal{H}_{23} - \mathcal{H}_{13}(\mathcal{H}_{22} - m_{\nu 1}^2), & X_2 &= \mathcal{H}_{13}\mathcal{H}_{23} - \mathcal{H}_{12}(\mathcal{H}_{33} - m_{\nu 1}^2), \\
Y_2 &= (\mathcal{H}_{11} - m_{\nu 2}^2)(\mathcal{H}_{33} - m_{\nu 2}^2) - \mathcal{H}_{13}^2, & Z_2 &= \mathcal{H}_{12}\mathcal{H}_{13} - \mathcal{H}_{23}(\mathcal{H}_{11} - m_{\nu 2}^2), \\
X_3 &= \mathcal{H}_{12}\mathcal{H}_{23} - \mathcal{H}_{13}(\mathcal{H}_{22} - m_{\nu 3}^2), & Y_3 &= \mathcal{H}_{12}\mathcal{H}_{13} - \mathcal{H}_{23}(\mathcal{H}_{11} - m_{\nu 3}^2), \\
Z_3 &= (\mathcal{H}_{11} - m_{\nu 3}^2)(\mathcal{H}_{22} - m_{\nu 3}^2) - \mathcal{H}_{12}^2. \quad (\text{C2})
\end{aligned}$$

The mixing angles among three tiny neutrinos can be defined as follows

$$\begin{aligned}
\sin \theta_{13} &= |(U_\nu)_{13}|, & \cos \theta_{13} &= \sqrt{1 - |(U_\nu)_{13}|^2}, \\
\sin \theta_{23} &= \frac{|(U_\nu)_{23}|}{\sqrt{1 - |(U_\nu)_{13}|^2}}, & \cos \theta_{23} &= \frac{|(U_\nu)_{33}|}{\sqrt{1 - |(U_\nu)_{13}|^2}}, \\
\sin \theta_{12} &= \frac{|(U_\nu)_{12}|}{\sqrt{1 - |(U_\nu)_{13}|^2}}, & \cos \theta_{12} &= \frac{|(U_\nu)_{11}|}{\sqrt{1 - |(U_\nu)_{13}|^2}}. \quad (\text{C3})
\end{aligned}$$

Acknowledgments

This work is supported by National Natural Science Foundation of China (NNSFC) (No.12075074), Natural Science Foundation of Hebei Province (A2023201040, A2022201022, A2022201017, A2023201041), Natural Science Foundation of Hebei Education Department (QN2022173), Post-graduate's Innovation Fund Project of Hebei University (HBU2024SS042), the Project of the China Scholarship Council (CSC) No. 202408130113. X. Dong acknowledges support from Fundação para a Ciência e a Tecnologia (FCT, Portugal) through the projects CFTP FCT Unit UIDB/00777/2020 and UIDP/00777/2020.

- [1] T2K Collab, Phys. Rev. Lett. **107** (2011) 041801; MINOS Collab, Phys. Rev. Lett. **107** (2011) 181802; DOUBLE-CHOOZ Collab, Phys. Rev. Lett. **108** (2012) 131801; DAYA-BAY Collab, Phys. Rev. Lett. **108** (2012) 171803; PoS HQL **2014** (2014) 019.
- [2] I. Girardi , S.T. Petcov , A.V. Titov, Nucl. Phys. B **894** (2015) 733-768.
- [3] P. Ghosh, S. Roy, J. High Energy Phys. **0904** (2009) 069.
- [4] P. Ghosh, P. Dey, B. Mukhopadhyaya, S. Roy, J. High Energy Phys. **1005** (2010) 087.
- [5] J. Li, PoS **EPS-HEP2023** (2024) 148
- [6] D. Adey, *et al.* [DayaBay] Phys. Rev. Lett. **121** (2018) 241805.
- [7] F. P. An, *et al.* [DayaBay] Phys. Rev. Lett. **108** (2012) 171803.
- [8] V. Cirigliano, K. Fuyuto, C. Lee, *et al.* J. High Energy Phys. **03** (2021) 256.
- [9] S. Navas *et al.* [Particle Data Group], Phys. Rev. D **110** (2024) no.3, 030001.
- [10] X.Y.Han, S.M.Zhao, L. Ruan *et al.* Eur. Phys. J. C **85** (2025) 2, 163.
- [11] A. Batra, P. Bharadwaj, S. Mandal *et al.* J. High Energy Phys. **07** (2023) 221.
- [12] N. Escudero, D.E.L. Fogliani, C. Munoz, *et al.* J. High Energy Phys. **12** (2008) 099.
- [13] E. Ma, Phys. Rev. D **73** (2006) 077301.
- [14] P. Minkowski, Phys. Lett. B **67** (1977).
- [15] P. Ghosh, P. Dey, B. Mukhopadhyaya *et al.* J. High Energy Phys. **05** (2010) 087; P. Ghosh, S. Roy, J. High Energy Phys. **04** (2009) 069.
- [16] S.M. Zhao, T.F. Feng, X.X. Dong *et al.* Nucl. Phys. B **910** (2016) 225-239.
- [17] T.F. Feng, X.Q. Li, Phys. Rev. D **63** (2001) 073006.

- [18] Y.L. Yan, T.F. Feng, J.L. Yang *et al.* Phys. Rev. D **97** (2018) no.5, 055036.
- [19] M. Dvornikov, Phys. Rev. D **111** (2025) no.5, 056009.
- [20] H.B. Zhang, T.F. Feng, L.N. Kou *et al.* Int. J. Mod. Phys. A **28** (2013) no.24, 1350117.
- [21] Y. Grossman, H.E. Haber, Phys. Rev. D **59** (1999) 093008.
- [22] U. Ellwanger, C. Hugonie, A.M. Teixeira, Phys. Rept. **496** (2010) 1-77.
- [23] G. Belanger, J.D. Silva, H.M. Tran, Phys. Rev. D **95** (2017) 115017.
- [24] V. Barger, P.F. Perez, S. Spinner, Phys. Rev. Lett. **102** (2009) 181802.
- [25] P.H. Chankowski, S. Pokorski, J. Wagner, Eur. Phys. J. C **47** (2006) 187.
- [26] J.L. Yang, T.F. Feng, S.M. Zhao, *et al.* Eur. Phys. J. C **78** (2018) 714.
- [27] J. Liu, Y.P. Yao, Phys. Rev. D **41** (1990) 2147; H. Simma, D. Wyler, Nucl. Phys. B **344** (1990) 283; S. Herrlich and J. Kalinowski, Nucl. Phys. B **381** (1992) 50.
- [28] P. Ghosh, P. Dey, B. Mukhopadhyaya, *et al.* J. High Energy Phys. **05** (2010) 087.
- [29] B. Dziewit, S. Zajac, M. Zralek, Acta Phys. Pol. B **42** (2011) 2509.
- [30] S. Navas *et al.*, Phys. Rev. D **110** (2024) 3, 030001.
- [31] CMS collaboration, Phys. Lett. B **716** (2012) 30.
- [32] ATLAS collaboration, Phys. Lett. B **716** (2012) 1.
- [33] ATLAS collaboration, Phys. Lett. B **796** (2019) 68.
- [34] P. Cox, C.C. Han, T.T. Yanagida, Phys. Rev. D **104** (2021) 075035.
- [35] M. V. Beekveld, W. Beenakker, M. Schutten, *et al.* SciPost Phys. **11** (2021) 3, 049.
- [36] M. Chakraborti, L. Roszkowski, S. Trojanowski, J. High Energy Phys. **05** (2021) 252.
- [37] F. Wang, L. Wu, Y. Xiao, *et al.* Nucl. Phys. B **970** (2021) 115486.
- [38] M. Chakraborti, S. Heinemeyer, I. Saha, Eur. Phys. J. C **81** (2021) 12.
- [39] M. Endo, K. Hamaguchi, S. Iwamoto, *et al.* J. High Energy Phys. **07** (2021) 075.
- [40] J. Zhang, J. Cao, JHEP **03** (2023) 072, [arXiv:2206.15317 [hep-ex]].
- [41] A. Abusleme, *et al.* [JUNO], Chin. Phys. C **46** (2022) 123001, [arXiv:2204.13249 [hep-ex]].
- [42] K.B. Luk, Reactor neutrino i_latest results from daya bay, June, 2022. 10.5281/zenodo.6683712.